Available online at www.sciencedirect.com
ScienceDirect
Journal of the European Ceramic Society 31 (2011) 2997–3002
www.elsevier.com/locate/jeurceramsoc

Mechanical characterization of porous $Ba_{0.5}Sr_{0.5}Co_{0.8}Fe_{0.2}O_{3-d}$

M. Lipinska-Chwalek [a], J. Malzbender [a,*], A. Chanda [b], S. Baumann [a], R.W. Steinbrech [a]

[a] *Forschungszentrum Jülich GmbH, IEK, 52428 Jülich, Germany*
[b] *Jadavpur University, Mechanical Engineering Department, Kolkata 32, India*

Received 10 May 2011; received in revised form 27 June 2011; accepted 2 July 2011
Available online 26 July 2011

Abstract

The mechanical stability of porous $Ba_{0.5}Sr_{0.5}Co_{0.8}Fe_{0.2}O_{3-d}$ (BSCF) material was investigated using depth-sensitive microindentation and ring-on-ring biaxial bending tests. The porous BSCF was characterized as potential substrate material for the deposition of a dense membrane layer. Indentation tests yielded values for hardness and fracture toughness up to a temperature of 400 °C, while bending tests permitted an assessment of elastic modulus and fracture stress up to 800 °C. In addition the fracture toughness was evaluated up to 800 °C measuring in bending tests the fracture stress of pre-indented specimens. The results proof that the indentation-strength method can be applied for the determination of the fracture toughness of this porous material. In comparison to dense material the values of the mechanical parameters were as expected lower but the temperature dependences of elastic modulus, fracture strength and toughness were similar to those reported for dense BSCF.

Keywords: Mechanical properties; Fracture; Strength; Perovskites; Membranes

1. Introduction

Perovskite materials of ABO_3 type (where A can be La, Sr, Ca, Ba and B can be Co, Fe) have been successfully introduced as cathodes for solid oxide fuel cells and are currently investigated as gas separation membranes.[1,2] In particular for oxygen transport membranes (OTMs) the advantage of the perovskite materials is their mixed ionic electronic conductivity (MIEC). Especially BSCF (Ba–Sr–Co–Fe-oxides) and LSCF (La–Sr–Co–Fe oxides) perovskites with different stoichiometries were found to have high oxygen permeation at elevated temperatures.[3,4] However, to permit a long term reliable operation at high temperatures and mechanical robustness of the gas separation setup not only the oxygen flux and chemical stability under operating conditions is of importance but also the mechanical strength needs to receive consideration. In fact, it has been shown that unlike many ceramics the thermo-mechanical properties of these perovskites are not monotonously changing with temperature. Their mechanical behaviour is strongly linked to the occurrence of phase changes. Also changes in the magnetic susceptibility have been reported that can affect oxygen transport and chemical expansion.[5–7]

A competitive technical application of OTM membranes with cryogenic processes requires a priori a high flux. The flux is a material specific parameter that depends in addition to the membrane thickness also on the surface activity. Hence an increase can be achieved by a reduction of the membrane thickness, by catalytic layers or by an increase of the surface area.[2] Under mechanical aspects the thickness reduction reaches its limit when handling related loads exceed the critical fracture stress of the material. An approach to stabilize a thin membrane is to deposit it as a layer on a mechanically supporting porous substrate.[2,8] Due to the thermal expansion mismatch significant residual stresses and unwanted warping effects can develop in layered composite materials.[2] In this respect a porous substrate made of the same material as the dense membrane appears to be advantageous. The mechanical reliability of such a bi-layered composite design clearly depends on mechanical stability and the structural integrity of membrane and substrate.

Besides the thermal expansion and the elastic behaviour of the layers, fracture strength and toughness are the mechanical properties that need to be known as a function of temperature.

* Corresponding author. Tel.: +49 2461 61 6964.
E-mail address: j.malzbender@fz-juelich.de (J. Malzbender).

0955-2219/$ – see front matter © 2011 Elsevier Ltd. All rights reserved.
doi:10.1016/j.jeurceramsoc.2011.07.002

Note that in the case of ceramic materials the fracture stress has to be assessed statistically, e.g. using characteristic strength and Weibull modulus. The two parameters permit a determination of the failure probability for any particular applied intrinsic or extrinsic stress level. Also note, that due to the statistical nature of failure-relevant-flaws, also the size of the component in real application needs to be considered in deriving the mechanical stress limits.[9]

Interestingly, the mechanical properties of porous perovskite support materials for dense membranes of the same composition have not received attention to date. This is in contrast to the many permeation studies and thermal/chemical expansion measurements of dense membrane materials.[5,6,10–14] The present work reports average values of key mechanical properties, in particular elastic modulus, fracture toughness and fracture stress of porous BSCF as a function of temperature.

2. Experimental

BSCF samples were provided by the IEK-1, Forschungszentrum Jülich GmbH. The samples were prepared by tape casting using slurries of BSCF powders supplied by Treibacher Industrie AG, Austria (for more details on sample preparation see Ref. [15]). The tape casted material foil was shaped into circular disc samples using a hollow punch. Subsequent sintering was performed at 1000 °C for 10 h applying optimized heating and cooling routines. Up to 600 °C a low heating rate (∼1 K/min) helped to burn out the organic components (debindering process). From 600 °C to maximum temperature the heating rate was 5 K/min. The same rate of temperature change was applied upon cooling. Thickness and diameter of the sintered samples was 0.80 ± 0.05 and ∼25 mm, respectively. The sintered discs were ground and subsequently polished to mirror finish for indentation tests while for the bending tests as-received samples without additional surface preparation were used. Light microscopy (LM) and scanning electron microscopy (SEM) were applied for the microstructural characterizations. The porosity of the samples was determined graphically from micrographs of the polished material cross-sections (Software Image-J).

The indentation hardness was measured as a function of temperature from RT to 400 °C (upper limit of the instrument) using a micro-Vickers indentation device (CSM, Switzerland). At room temperature the apparent elastic modulus was determined from the indentation load–penetration curve following the Oliver and Pharr procedure.[16] For the tests at elevated temperatures, a heating rate of 3 K/min and a dwell time of 1 h were used. The maximum indentation load was systematically varied from 2 N to 10 N. Interference between the indentation cracks and stress field around subsequent indentations was avoided by separating indents by at least three times the indentation size. Loading and unloading curves were recorded through built-in data acquisition software, permitting also the calculation of a plasticity parameter (ratio of final depth to maximum depth). For each load, at least ten indentations were performed. The diagonals of the impressions were used for hardness calculation and the crack lengths served as the basis for the fracture toughness evaluation. The measurements were performed using a light microscope (CSM, Switzerland). The analysis was limited to cases where the indentation crack path was not influenced by pores. From the crack length, as determined by image analysis software, the indentation fracture toughness (K_{IM} values) was derived. The respective relationship for calculating K_{IM} was selected in accordance to the actual subsurface crack shape. The subsurface contour of the indentation cracks was studied with a stereo-zoom and a scanning electron microscope (SEM, LEO1530, Zeiss, Germany).

Elastic modulus and fracture stress were determined using bi-axial ring-on-ring bending test after ASTM C1499. Details of the ring-on-ring fracture tests along with the equations used for evaluation have been reported elsewhere.[6,7]

Complementary, the fracture toughness was evaluated using the "indentation strength method" (ISM, K_{ISM} values).[17] The discs were subjected to a surface impression and the indented surface was subsequently tensile loaded in a bi-axial ring-on-ring bending test until fracture occurred.[18] The use of the indentation-strength method permitted to measure the apparent fracture toughness over the entire range from room to operation temperature of the membrane material. Similar to the testing procedure of fracture stress and elastic modulus the biaxial loading of pre-indented samples followed the ASTM standard (C1499-05).

All bi-axial bending tests were carried out in air at room temperature (RT), 200 °C, 400 °C, 600 °C and 800 °C. At elevated temperatures, a heating rate of 8 K/min was used and a dwell time of 1 h was chosen to reach thermal equilibrium before testing. The central displacement of the specimen was recorded with a sensor that contacted the lower surface of the sample (tensile surface). The loading rate was 100 N/min in all tests. All investigated samples fractured at a displacement value far smaller then half of the specimen thickness, which is a prerequisite for the linear elastic stress–strain analysis (ASTM C1499-05).

3. Results and discussion

Fig. 1 shows a typical SEM micrograph of the porous BSCF material in the as-sintered state. The porosity measurement yielded a value of $38 \pm 1\%$ for both surface and cross-section. Pores were often interlinked and the shape of the individual pores was generally nodular. The average grain size was 5 ± 2 μm.

The apparent elastic modulus (stiffness) of porous BSCF determined at RT from ring-on-ring bending test data was 33 ± 5 GPa. The temperature dependence is given in Fig. 2, where the elastic modulus is normalized with respect to the RT value. For comparison also normalized values for a nominal dense material are shown (porosity of 4.5%, RT elastic modulus: 63 ± 3 GPa[5]). Although the absolute values of the elastic modulus are ∼50% lower for the porous material, the temperature dependency is similar to that of the dense material. An initial decrease with increasing temperature and a minimum at ∼200 °C are followed by a subsequent recovery. Above 400 °C the elastic modulus behaves as expected for ceramic materials, i.e. it decreases slightly with increasing temperature. For dense BSCF, it has been recently reported that the minimum at

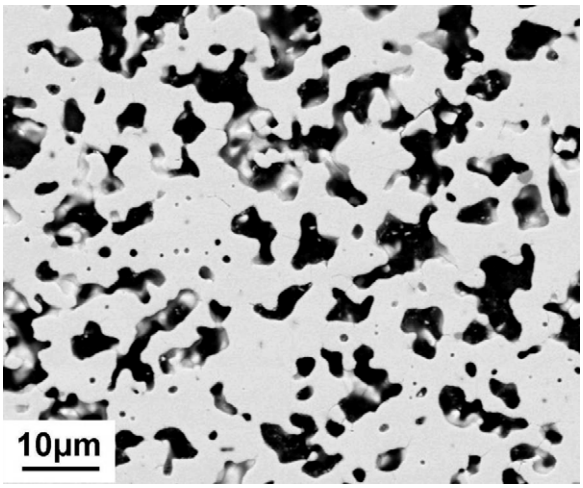

Fig. 1. SEM image of polished cross-section of as-sintered porous BSCF material.

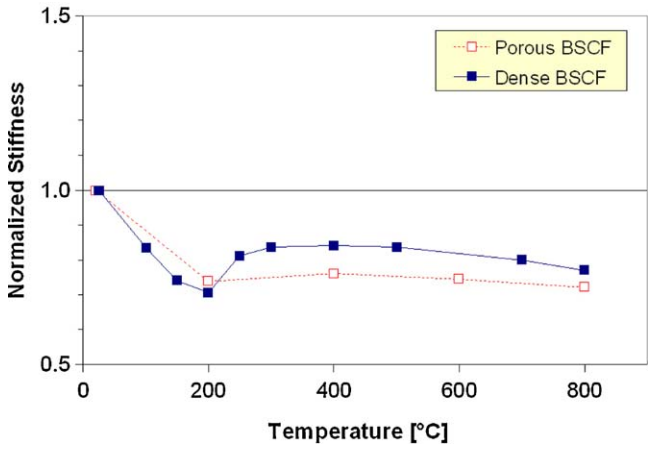

Fig. 2. Comparison of the temperature dependence of the elastic modulus for porous and dense BSCF.[19] Both data sets are normalized with respect to the RT values.

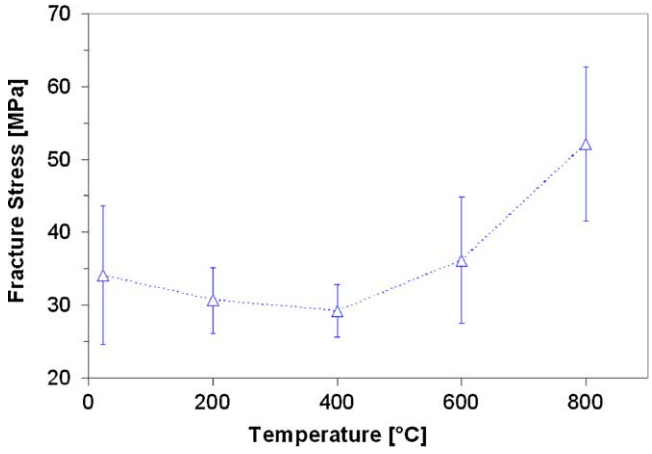

Fig. 3. Fracture stress of porous BSCF as a function of temperature.

around 200–250 °C is associated with a saturation of Co^{3+} spin transition (Fig. 3).[5]

The average fracture stress of the porous BSCF (RT: average strength $\sigma = 34$ MPa, characteristic strength $\sigma_{char} = 38$ MPa, Weibull modulus $m = 4$) also decreases initially with temperature but exhibits a broader minimum and finally at high temperature it becomes even larger than the initial RT value. Considering the mechanical reliability of the porous membrane substrate, the material appears to be more susceptible to fracture at lower temperatures. Also the fracture stress (~50 MPa) is significantly lower than that of dense BSCF at 800 °C (~80 MPa).[5]

The elastic modulus determined by means of the indentation technique was 38 ± 3 GPa (1 N indentation load), which agrees within the limits of uncertainty with the average value obtained by the bi-axial bending tests. For all indentation testing temperatures (RT – 400 °C) no signs of pile-up were observed around the impressions that might question the use of the relationships to determine elastic modulus and hardness. In most of the cases, at RT as well as elevated temperatures, the value of the plasticity parameter was less than 0.7, the threshold above which pile-up around the indenter might be expected.[20]

The mechanical properties determined by the indentation tests showed a large scatter due to the local influence of pores on the individual tests. In this context, it may be noted that the indentation energy is partly consumed in collapsing the pores below the indentation. Like for other ceramic material, the hardness decreased with increasing indentation load (Fig. 4). This indentation size effect might be associated with the increasing probability to include pores in the deformed volume of the impression at higher loads. However, the hardness decrease with increasing load was rather small (20%, for a factor >10 load increase). The average RT hardness of the as-sintered material was 0.87 ± 0.03 GPa for a load of 10 N. The deformed area of $\sim 11{,}300 \pm 400\ \mu m^2$ at this load was already significantly larger than pore and grain sizes and hence the value appears to be characteristic for the global behaviour of the material.

A similar indentation size effect was also observed for tests carried out at elevated temperatures (Fig. 5). The overall decrease of the hardness from RT to 400 °C was of the order of 30–40%. Since hardness is a parameter that depends on elastic and inelastic deformation, the decrease with increasing temperature is partly a result of the decreasing elastic modulus (Fig. 2). Again the behaviour is similar to that reported for dense

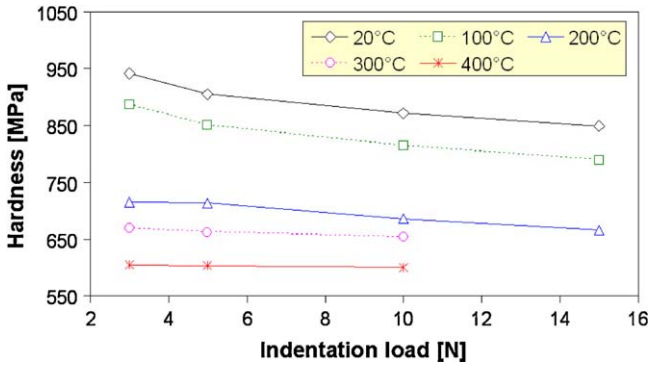

Fig. 4. Indentation load dependence of the hardness.

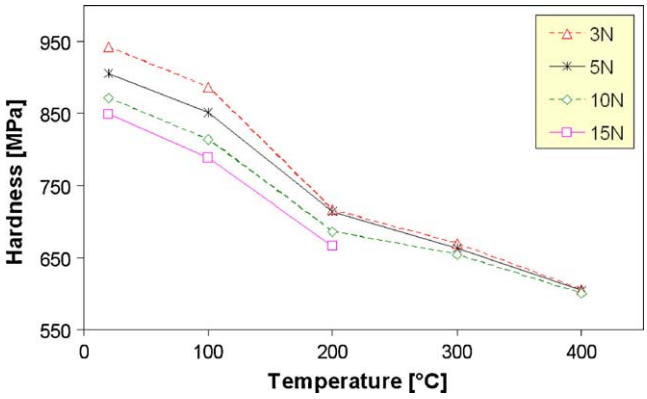

Fig. 5. Dependence of the hardness on the indentation temperature (load 10 N).

BSCF material[19]; however the porosity results in almost 80% lower absolute values. The hardness values used to determine the fracture toughness by the indentation-strength method at elevated temperatures were extrapolated from these data. Note that, although important for the evaluation of the fracture toughness, in the application as a substrate for dense membrane layers it is not a crucial parameter, rendering the lower values for the porous material rather uncritical.

Applying the indentation-strength method (ISM) discrete boundary conditions for the indentation cracks have to be satisfied.[17] The indentation cracks should be large enough to act as fracture origin; and as a second requirement, it was suggested that the maximum crack depth should not exceed 1/10 of the specimen thickness. Furthermore, the toughness evaluation is based on the assumption that the crack has a radial-median contour. The crack length introduced by the indent reached already ~0.16 of the sample thickness at a load of 5 N. However, higher loads were chosen for the analysis since in the subsequent ring-on-ring bending tests, the samples did only fracture from the indentation-introduced cracks at higher loads. The fracture toughness values evaluated by the ISM for pre-indentation loads of 10 and 15 N agreed within the accuracy of the measurement. Hence in this load regime the evaluation did not depend on the depth of the initial indentation cracks. To improve the statistical relevance of the failure origin from the indentation cracks the pre-indentation load of 15 N was selected. For the subsequent toughness determination only data were taken into account where the indentation cracks caused the sample fracture,[21] which was confirmed by fractographic analysis.

Fracture surfaces (Fig. 6) revealed a mixed mode fracture surface in a semi-circular zone directly underneath the impression (dotted line) where compressive stresses predominated during the indentation process. Further away from the impression, where tensile stress was present during the unloading sequence of the indentation, predominantly transgranular fracture was present.

The reduction of the average fracture stress due to the pre-indentation cracks of $c_0 = 160\,\mu m$ was 20–30% for the entire temperature range, verifying again that indentation cracks were the failure sources in these bending tests. The product of fracture stress σ_f and the indentation load $P^{1/3}$ was found to be constant for indentation loads of ≥ 10 N (Fig. 7), which justifies the application of the indentation-strength method, since[17]:

$$K_{ISM} = A \cdot \left(\frac{E}{H}\right)^{1/8} [\sigma_f P^{1/3}]^{3/4} \quad (1)$$

During the bending experiment the indentation induced residual stress field results in a subcritical (stable) growth of the indentation induced crack. This effect is considered by the calibration factor A, which was derived experimentally as 0.59 in Ref. [22]. The basis of this calibration value is that the ratio between the maximal crack length after stable crack growth c_m (just before catastrophic specimen failure) and the initial indentation induced crack length c_0 is $(c_m/c_0)^{3/8} = 1.34^{3/8}$. Note that this analysis relies on the combined interaction of residual-indentation and

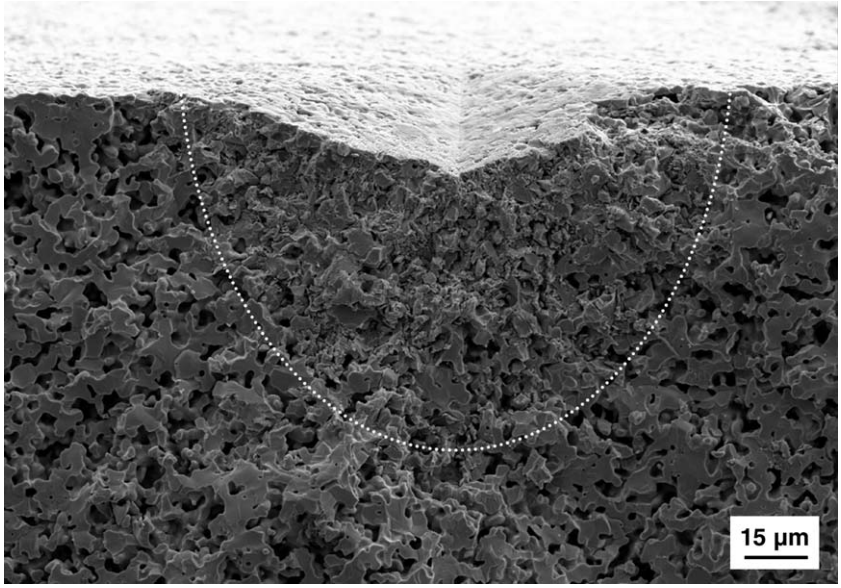

Fig. 6. SEM images of the fracture surface after biaxial bending test. Fracture originated from indentation-introduced crack. Mixed mode fracture in the deformation zone underneath impression and predominantly transgranular fracture mode in the zone of tensile stresses.

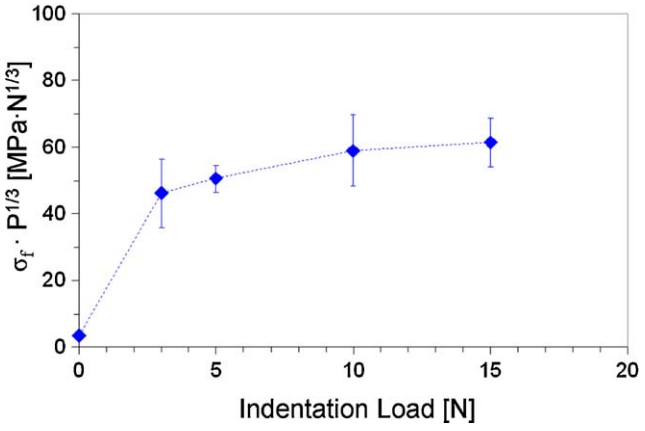

Fig. 7. Indentation-load dependence of the product of fracture stress σ_f and the indentation load $P^{1/3}$.

Table 1
Crack extension ratio as a function of temperature.

	Temperature [°C]				
	23	200	400	600	800
c_m/c_0	1.32	1.38	1.05	1.02	1

applied-bending stress. In fact, observation of the fracture surfaces of the porous BSCF samples revealed a different ratio. Hence, based on experimental results, corrected A factors had to be calculated for the individual testing temperatures.

For this purpose, multiple indents (13) were placed on polished sample surfaces with a load of 10 N. The indents were positioned close to the centre of the specimens inside the area where a constant tensile stress field could be expected in the subsequent ring-on-ring bending test. Interference between the indentation cracks and the stress field around other indentations was avoided by adequate spacing. In order to determine the amount of stable crack, the size of the indentation cracks was measured before and after bending tests (c_0 and c_m, respectively). The results are summarized in Table 1.

Based on these values, the fracture toughness of porous BSCF is plotted in Fig. 8 as a function of temperature. At RT an average fracture toughness of $K_{ISM} = 0.58\,MPa\,m^{0.5}$

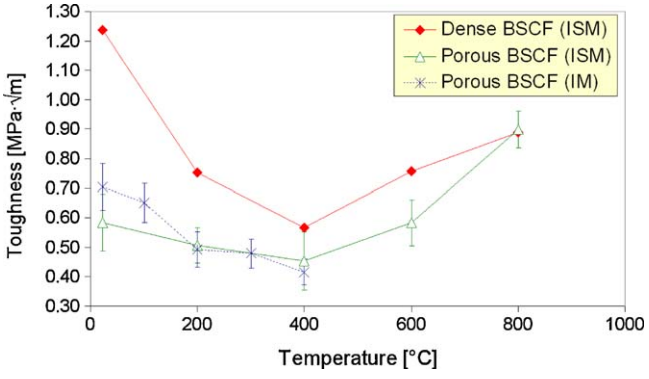

Fig. 8. Temperature dependence of fracture toughness. Comparison of porous BSCF evaluated by means of indentation-strength and standard indentation techniques with values for dense BSCF.[19].

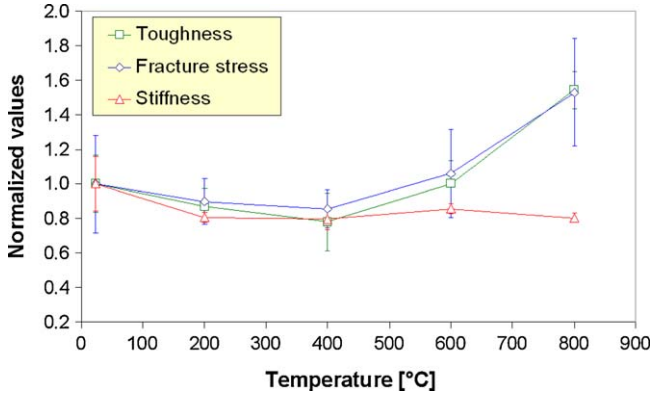

Fig. 9. Comparison of normalized values of the elastic modulus, fracture strength (both obtained using biaxial bending) and toughness (indentation-strength method) of porous BSCF.

(uncertainty 17%) was obtained. The toughness exhibits a flat minimum (~0.50 MPa $m^{0.5}$) between ~200 °C and 400 °C and then increases to an average value of ~0.9 MPa $m^{0.5}$ at 800 °C. For comparison, fracture toughness values for dense BSCF from Ref. [19] are also included in Fig. 8. The data for the dense material were corrected using the same correction procedure as applied for porous BSCF. Note that in the previous work[19] the correction for dense BSCF was not included, which changes the data for dense BSCF slightly (maximum change around 10%). In comparison with dense BSCF[19] the fracture toughness is lower up to 600 °C. At 800 °C the values for porous and dense material became similar.

Up to 400 °C the fracture toughness was also determined from the length of indentation cracks based on the relationships given in Ref. [23]. The indentation crack results (K_{IM} values) are in good agreement with the toughness derived from the indentation-strength method (Fig. 8).

Finally, Fig. 9 compares normalized elastic modulus, fracture stress and fracture toughness values as a function of temperature. All mechanical parameters decrease up to 400 °C. Contrary to fracture stress and toughness the elastic modulus remains rather constant at higher temperatures. Fracture stress and toughness have similar temperature dependencies up to 800 °C. Since toughness is proportional to the product of strength ad the square root of the defect size the correlation is to be expected when the failure relevant defect population is temperature invariant. Fig. 9 also provides information about the average critical strain as a function of temperature. Since the ratio of fracture stress and elastic modulus remains stable up to 600 °C, a constant strain value of $0.10 \pm 0.03\%$ can be estimated. Note also that both parameters have the same proportionality to the porosity. However, as a consequence of the different temperature dependency of fracture stress and elastic modulus the strain almost doubles to $0.19 \pm 0.03\%$ at 800 °C.

4. Conclusion

Elastic modulus, fracture stress and fracture toughness have been presented for a porous BSCF considered as a possible substrate material for thin BSCF oxygen transport

membranes. The three characteristic mechanical parameters show a minimum at intermediate temperatures. Compared to dense BSCF, fracture stress and elastic modulus of the porous BSCF (porosity ∼38%) are ∼50–60% lower for the entire temperature range. At 800 °C the fracture toughness values of porous and dense material are similar.

The fracture toughness has been determined using the indentation-strength method. In general it is difficult to derive the toughness of porous materials using standard methods based on the length measurement of indentation induced cracks. In fact, it appears that for the investigated porous BSCF material the indentation-strength method, which does not require the extensive notching procedure of standard specimens [ASTM C1421-10], can be used conveniently. Even at elevated temperatures the fracture toughness has been determined from bending-strength measurements of pre-indented specimens.

Acknowledgements

Financial support from the Federal Ministry of Economics and Technology via the MEM-OXYCOAL project (grant no. 0327803) is gratefully acknowledged. The authors would like to thank W.A. Meulenberg and F. Schulze-Küppers for preparing and providing the porous BSCF specimens and R. Küppers for his experimental and technical support in the mechanical tests. In addition, most valuable SEM investigations provided by E. Wessel are gratefully acknowledged.

References

1. Skinner SJ, Kilner JA. *Mater Today* 2003;**6**:30–7.
2. Sunarso J, Baumann S, Serra JM, Meulenberg WA, Liu S, Lin YS, et al. *J Membr Sci* 2008;**320**:13–41.
3. Vente JF, Haije WG, Rak ZS. *J Membr Sci* 2006;**276**:178–84.
4. Shao ZP, Yang WS, Cong Y, Dong H, Tong JH. *J Membr Sci* 2000;**172**: 177.
5. Huang BX, Malzbender J, Steinbrech RW, Singheiser L. *J Membr Sci* 2010;**359**:80–5.
6. Huang BX, Malzbender J, Steinbrech RW, Grychtol P, Schneider CM, Singheiser L. *Appl Phys Lett* 2009;**95**:051901.
7. Malzbender J, Huang B, Mönch J, Steinbrech RW. *J Mater Sci* 2010;**45**:1227.
8. Shao ZP, Xiong GX, Tong JH, Dong H, Yang WS. *Sep Purif Technol* 2001;**25**:419.
9. Malzbender J, Steinbrech RW. *J Eur Ceram Soc* 2008;**28**(1):247–52.
10. Wei B, Lu Z, Huang XQ, Miao JP, Sha XQ, Xin XS, et al. *J Eur Ceram Soc* 2006;**26**:2827.
11. Li DC, Liu W, Zhang HL, Jiang GS, Chen CS. *Mater Lett* 2004;**58**:1561.
12. van Veen AC, Rebeilleau M, Farrusseng D, Mirodatos C. *Chem Commun* 2003:32.
13. Itoh T, Shirasaki S, Fujie Y, Kitamura N, Idemoto Y, Osaka K, et al. *J Alloys Compd* 2010;**491**:527.
14. Itoh T, Nishida Y, Tomita A, Fujie Y, Kitamura N, Idemoto Y, et al. *Solid State Commun* 2009;**149**:41.
15. Betz M, Baumann S, Meulenberg WA. Ceramic membranes for oxyfuel power plants. In: *Fourth international conference on clean coal technology (CCT2009)*. 2009., ISBN 978-92-9029-467-2.
16. Oliver WC, Pharr GM. *J Mater Res* 1992;**7**:1564.
17. Chantikul P, Anstis GR, Lawn BR, Marshall DB. *J Am Chem Soc* 1981;**64**:539.
18. Lawn BR, Evans AG. *J Am Chem Soc* 1980;**63**:574.
19. Chanda A, Huang BX, Malzbender J, Steinbrech RW. *J Eur Ceram Soc* 2011;**31**:401–8.
20. Bolshakov A, Pharr GM. *J Mater Res* 1998;**13**(4):1049.
21. Cook RF, Lawn BR, Fairbanks CJ. *J Am Soc* 1985;**68**:604.
22. Zhang J, Ardell AJ. *J Mater Res* 1991;**6**:1950–7.
23. Anstis GR, Chantikul P, Lawn BR, Marshall DB. *J Am Ceram Soc* 1981;**64**:533.